

ARTICLE OPEN



Optimization, kinetics and thermodynamics studies for photocatalytic degradation of Methylene Blue using cadmium selenide nanoparticles

Parvin Gharbani¹✉, Ali Mehrizad² and Seyyed Amir Mosavi³

In this study, the photocatalytic degradation of Methylene Blue was investigated using CdSe nanoparticles. CdSe nanoparticles were synthesized via a simple method and were characterized by FTIR, XRD, FESEM, BET, DRS and EDS techniques. The photocatalytic performance of the CdSe nanoparticles was optimized using Response Surface Methodology (RSM) under visible light. The independent variables involved initial pH, MB concentration, photocatalyst dosage, and irradiation time were evaluated and the optimum photodegradation efficiency of MB dye removal was achieved ~92.80% at pH = 8, 20 mgL⁻¹ of MB concentration, 0.02 g 50 mL⁻¹ of CdSe dosage, and 20 min of irradiation time. Also, the photodegradation of MB by CdSe is obeyed pseudo-first-order kinetic model ($k = 0.038 \text{ min}^{-1}$). The thermodynamic results revealed that the photocatalytic degradation of MB is spontaneous and endothermic. Also, the evaluation of various scavengers confirmed that the MB photodegradation was mainly done by photogenerated holes and hydroxyl radicals.

npj Clean Water (2022)5:34; <https://doi.org/10.1038/s41545-022-00178-x>

INTRODUCTION

Colored effluents produced by various industries, including textile, paper, printing, rubber, and plastic industries can cause many significant problems to the environment, if discharged to the environment before treatment¹. Discharge of such effluents to receiving waters causes toxicity to ecosystems as well as the possibility of bioaccumulation in the environment². Dyes are stable chemically and due to having stable complex chemical structures can remain without change in the environment for a long time and cause turbidity and unpleasant odor in water³. Methylene Blue dye (MB) (Supplementary Fig. 1) is a multi-core aromatic ($M = 319.85 \text{ gmol}^{-1}$; $C_{16}H_{18}N_3S$) that not only causes acute toxic effects but also induces serious health problems such as shortness of breath, chest pain, burning sensation, nausea, vomiting and diarrhea⁴. There are many techniques for the removal of dyes from water and wastewaters such as adsorption, biodegradation, ionic exchange, fenton reactions, and advanced oxidation processes⁵. The advanced oxidation processes (AOPs) are based on the oxidation of the water pollutants using powerful oxidants such as H₂O₂, ozone, photocatalysts, ultraviolet radiation and etc. The photocatalytic process uses a renewable energy source in the treatment of pollutants and can significantly reduce highly toxic compounds to less harmful compounds. so, it is an effective, environmentally friendly, and economic process⁶.

The removal and decomposition of organic pollutants in the photocatalytic process is based on the excitation of the electrons from the valance band and their transfer to the conduction band. Therefore, the transfer of electrons causes a hole in the valance band and the production of hydroxyl radicals⁷. Photocatalysts as semiconductors catalyze many types of reactions such as water decomposition, hydrogen transfer, metal deposition, disinfection, and detoxification of water, and removal of contaminants⁸. Different metal oxide semiconductors such as TiO₂, ZnO, CuO, CuO₂, and WO₃ are the most common catalysts that are widely

used to degrade organic compounds due to their unique properties such as high photocatalytic activity and high optical and chemical stability⁹. However, these catalysts have challenges, including low quantum performance, wide bandgap energy, low conductivity, toxic effect, optical corrosion, and recombination rate⁵. In recent years, extensive researches have been carried out in II–IV semiconductors. Unique optical and electrical properties of ZnO, CdS, CdSe, ZnSe, and ZnS semiconductors have found broad applications especially in nanoscale¹⁰.

CdSe is one of the most important semiconductors in the construction of nanostructured solar cells due to its optoelectronic properties. In addition to applications in laser diodes, catalysts, light-emitting diodes, solar cells, and biological labels, CdSe nanoparticles can play an important role as a photocatalyst with regulated bandgap energy¹¹. Various methods have been proposed for the synthesis of CdSe nanoparticles including sonochemistry, electrochemical deposition, sol-gel, micro and nanoemulsions, hydrothermal, solvothermal methods and etc¹².

Design-Expert provides powerful tools for providing an ideal experiment on a process, mixture, or combination of factors and components. The major types of Design-Expert are: Full Factorials, Fractional Factorials, Screening Experiments, Response Surface methodology and EVOP(evolutionary operations). Response Surface methodology is one of the two major DOE techniques for optimizing processes. Compared to classical techniques, RSM can both evaluate the interactions between the operational variables tested and reduce the number of experiments¹³. Recently, the design of experiments and analysis of results using response surface methodology (RSM) is developed in many studies^{14–17}. RSM is a mathematical and statistical method that is applied to design experiments, optimization and study the effect of independent variables on the response that can lead to a purposeful and reliable conclusion.

¹Department of Chemistry, Ahar Branch, Islamic Azad University, Ahar, Iran. ²Department of Chemistry, Tabriz Branch, Islamic Azad University, Tabriz, Iran. ³Department of Chemical Engineering, Ahar Branch, Islamic Azad University, Ahar, Iran. ✉email: p-gharbani@iau-ahar.ac.ir

The aim of this work is a facile synthesis of CdSe photocatalyst via a thermal treatment method. The advantage of this method is flexibility, cheapness, ease, reproducibility, and synthesis of high purity nanoparticles without the use of additional chemicals. Then, the response surface methodology was applied to model and recognize the effect of independent variables on the removal of MB and to optimize the removal process using the photocatalytic process under visible light in a batch system. This method provides a logical distribution of design points throughout the design area and measures the adequacy of the model by performing a fitting weakness test¹⁸. The effects of four independent variables including, initial pH, irradiation time, initial MB concentration, and photocatalyst dosage were investigated. RSM was used in order to extract the model, find the interactions of the variables, and optimize the process¹⁹. The kinetic and thermodynamic and the effects of scavengers have also been studied.

RESULTS AND DISCUSSION

Characterization of CdSe

Figure 1a shows the FTIR spectra of prepared CdSe. The observed peaks at 3414, 2954, and 1642 cm^{-1} correspond to N-H, C-H, C=O stretching vibrations, respectively. Also, bending vibrations of C-H in the methylene group are seen at 1438 cm^{-1} . The peak located at 1111 cm^{-1} is also related to the vibrations of the C-C ring and the peak at 603 cm^{-1} corresponds to the bending of C-N=O^{20,21}.

The XRD pattern of prepared CdSe is presented in Fig. 1b. According to the synthesized CdSe was almost in crystalline form and the observed peaks correspond to the plates of hexagonal structure (010), (002), (011), (012), (110), (013), (020), (112), (021), (004), (022), (014), (023), (120), (121), (114), (015), (122), (024), (030), (031), (123), (032), (006), (025), (016), (124), (033) (JCPDS file No: 98-009-4990) of CdSe (Supplementary Table 1)²². Using Eq. (16) and

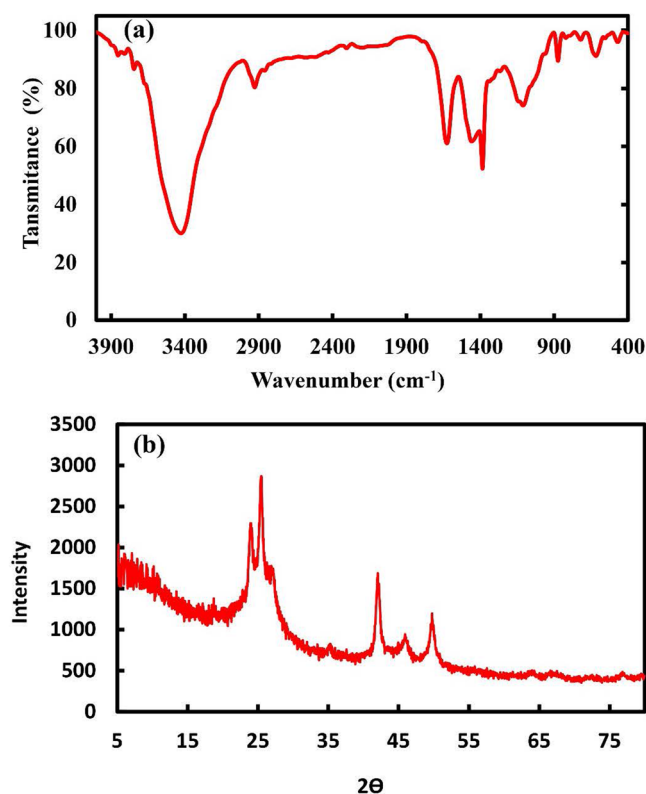


Fig. 1 Fourier transform infrared (FTIR) and X-ray powder diffraction (XRD) of CdSe nanoparticles. **a** FTIR and **b** XRD.

(17), theoretical density and specific surface area of CdSe were obtained 3.21 gcm^{-3} and 26.70 cm^2g^{-1} , respectively. The results showed that the synthesized CdSe has a high surface area and so it has a greater ability to provide photooxidation of electron-hole pairs inactive sites. The surface morphology of synthesized CdSe was investigated with FESEM (Fig. 2a). The FESEM analysis shows the formation of spherical-shaped CdSe nanoparticles with an average size of about 70 nm. So, the nanometer particle size of the synthesized CdSe is confirmed. EDS analysis of the CdSe was also used to identify the elemental composition of synthesized CdSe. Figure 2b indicates the presence of 15.7% Cd and 84.3% Se elements in the sample confirming the formation of CdSe. Also, the Se/Cd ratio was obtained about 5.36. BET analysis was used to determine the specific surface area and Supplementary Fig. 2 shows N_2 adsorption-desorption isotherms of the CdSe nanoparticles. According to IUPAC classification, the synthesized CdSe nanoparticles belong to II type isotherm indicating a non-porous or microporous structure. Also, the specific surface area for CdSe was obtained at about 26.71 m^2g^{-1} , that confirms the high active surface for prepared CdSe.

One of an is an important parameter in photocatalysts is finding the band gap from the UV-Vis absorbance of photocatalyst¹. UV-Vis Drs technique and the Kubelka-Munk equation were used to study optical properties and calculate the bandgap of CdSe, respectively.

From the UV-Vis spectrum (Fig. 3a) the band gap value (Fig. 3b) of CdSe was obtained about 2.55 eV, which confirms the high photocatalytic properties of the synthesized CdSe. So, it can be used as a strong photocatalyst in the visible region due to the generation of high electron-hole pairs.

Results of photocatalytic degradation

30 experiments (including 5 central points) were performed for selected 4 independent factors at 5 levels by CCD design and results are presented in Supplementary Table 2. According to, the maximum and minimum removal of MB were 96.98 and 57.98%, respectively.

The coefficients of parameters were analyzed using ANOVA (Table 1). F-value is used to compare the variance of the model with the remaining variance. As seen in Table 1, F-value = 99.64 confirms the significance of the model and indicates the performance of the model. On the other hand, the prob $P > F$ less than 0.0001 indicates the model was statically significant. Therefore, a quadratic polynomial equation was used to predict the efficiency of photocatalytic removal of MB as a function of independent factors (Eq. 1):

$$R = +77.38 + 1.36A + 0.64B + 1.88C + 2.19D - 2.28AB - 4.48AC + 6.37AD - 5.54BC - 2.10BD + 2.01CD + 0.35A^2 + 0.02B^2 + 0.28C^2 - 0.39D^2 \quad (1)$$

Here, A, B, C, and D are coefficients of linear factors, A^2 , B^2 , C^2 & D^2 are coefficients of quadratic factors and AB, AC, AD, BC, BD & CD are coefficients of interaction factors.

Prob $P > F$ values less than 0.05 of A (MB concentration), C (initial pH), D (irradiation time) factors also indicate the significant effect of these factors. On the other hand, the P -value of AB, AC, AD, BC, BD, CD interactions, was less than 0.05, so all have significant impacts on the model. In the case of quadratic forms, none of them had no significant effects on the MB removal efficiency and could be eliminated.

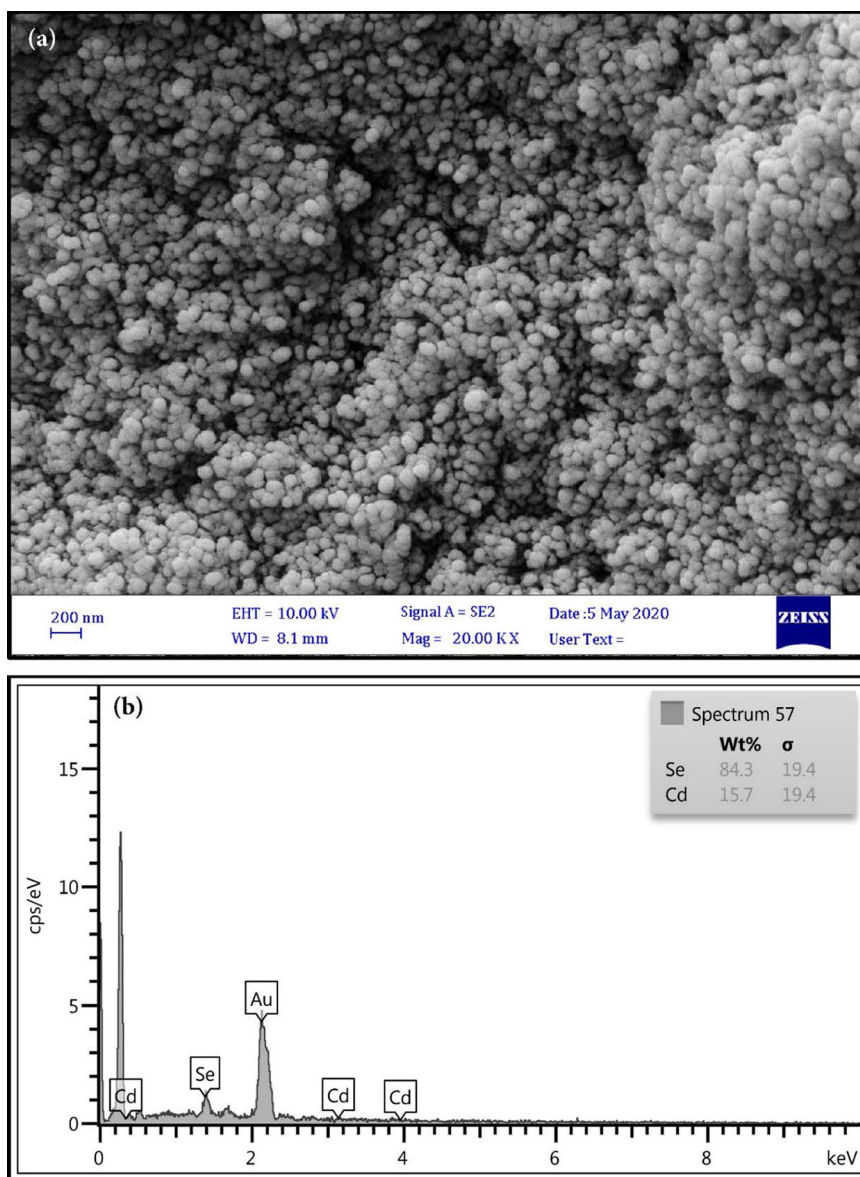


Fig. 2 Field emission scanning electron microscopy (FESEM) and Energy Dispersive Spectroscopy (EDX) of CdSe nanoparticles. **a** FESEM and **b** EDX.

As result of Table 1 and elimination of insufficient factors, Eq. (1) was simplified as Eq. (2):

$$R = +77.38 + 1.36A + 1.88C + 2.19D - 2.28AB - 4.48AC + 6.37AD - 5.54BC - 2.10BD + 2.01CD \quad (2)$$

Also, the values of R^2 and R^2_{adj} were 0.984 and 0.9799, respectively, and quite close to 1, confirming that the obtained model can predict MB removal efficiency. The F-value of lack of fit was 0.87, indicating that it was not significant, and the model is best fitted with the experimental data. Adeq Precision shows the signal-to-noise ratio and indicates the efficiency of the model for predicting the response, which is more favorable than 4²³. In this model, the number 46.581 confirms a sufficient signal.

Validity of the model

Validation of a model in the analysis of experiments depends on some assumptions, such as normal distribution of residuals, the variance of constant (∂^2), and the independence of the residues from each other²³. Figure 4a shows a graph of the actual values versus the predicted values. Normal distribution of data in a straight line confirms that the errors are properly distributed. The plot of residual values versus the predicted ones is shown in Fig. 4b. It indicates a random distribution without significant trends invariance. The level of coverage under Chi-square statistics for Bartlett's test was also zero, which indicates the appropriate status of this indicator (if the appropriate status is determined, the area covered by statistics is less than 5%). Also, the Internally Studentized Residuals diagram of the model in Fig. 4c shows no unusual points. The residual normal diagram of the model in Fig. 4d. confirms the residues follows the normal distribution.

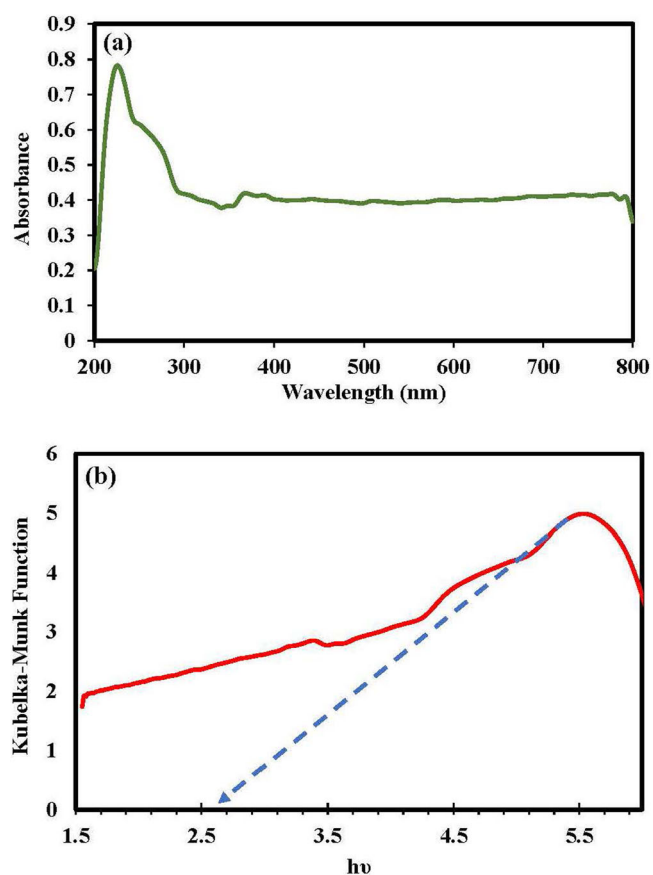


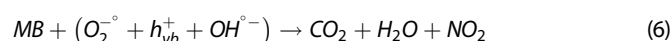
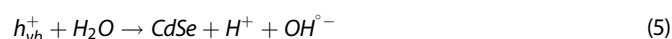
Fig. 3 Ultraviolet/Visible (UV-Vis) spectrum and Diffuse reflectance spectroscopy (DRS) of CdSe nanoparticles. **a** UV-Vis and **b** DRS.

Two-factor plots

Three-dimensional diagrams analyze the interaction between variables in MB photocatalytic removal, as shown in Fig. 5a and b. Figure 5a shows that the removal percentage of MB increases from 69.70% to 81.57% by increasing the photocatalyst dosage from 0.01 to 0.05 g 50 mL⁻¹. In fact, by increasing photocatalyst dosage, more active sites were increased, and more electron-hole pairs were generated. Subsequently, more active hydroxyl radicals are generated that enhance the mass transfer and photocatalytic degradation of MB. Meanwhile, by increasing photocatalyst dosage, more available surface area is generated. Both phenomena improved the removal of MB⁸. As shown in Fig. 5a, MB decomposition increases by increasing MB concentration (5–25 mg L⁻¹) from 69.70 to 85.52%. The initial dye appears to provide the driving force to overcome the mass transfer resistance between CdSe and MB, and the dye molecules adsorbed on the CdSe surface are play the main role in dye degradation²⁴. The effect of irradiation time on photodegradation of MB was investigated and the results are shown in Fig. 5b. It has been observed that with increasing irradiation time, MB degradation increases¹⁶. In fact, due to the availability of many active sites, the rate of destruction increases. Following an increase in irradiation time, the photocatalyst is exposed to visible light for a long time and creates more radicals for the degradation of MB. One of the key factors in the photocatalytic process is pH. It affects the surface charge of the photocatalyst²⁵. Here, the effect of pH on MB degradation in the range of 2–10 is studied. As result, degradation efficiency is increased with increasing pH. The relationship between the pH of the solution and MB removal percentage is shown in Fig. 5b. The results confirmed that the degradation of MB is approximately 88.95 % at pH = 10, while the degradation efficiency of less than 72.41% was

Table 1. Analysis of variance.					
Source	Sum of Squares	df	Mean Square	F Value	p-value Prob > F
Model	1944.2	14	138.87	99.64	<0.0001
A-Dye concentration	44.61	1	44.61	32.01	<0.0001
B-Dosage	9.84	1	9.84	7.06	0.0179
C-pH	85.16	1	85.16	61.11	<0.0001
D-Time	114.8	1	114.8	82.37	<0.0001
AB	83.49	1	83.49	59.91	<0.0001
AC	320.86	1	320.86	230.22	<0.0001
AD	648.34	1	648.34	465.2	<0.0001
BC	490.73	1	490.73	352.11	<0.0001
BD	70.85	1	70.85	50.84	<0.0001
CD	64.44	1	64.44	46.24	<0.0001
A^2	3.38	1	3.38	2.43	0.1401
B^2	0.023	1	0.023	0.017	0.8988
C^2	2.08	1	2.08	1.49	0.2407
D^2	4.19	1	4.19	3.01	0.1034
Residual	20.91	15	1.39		
Lack of Fit	13.29	10	1.33	0.87	0.602
Pure Error	7.61	5	1.52		
Cor Total	1965.11	29			
Std. Dev.	1.18	R-Squared	0.9894		
Mean	77.59	Adj R-Squared	0.9794		
C.V. %	1.52	Pred R-Squared	0.9555		
PRESS	87.52	Adeq Precision	46.581		

obtained at pH=2, due to the amphoteric nature of most semiconductor oxides. The physics of the semiconductor surface significantly depends on the pH of the solution and the dimensions of the agglomeration. The relationship between pH and photocatalytic degradation can be described as the pH_{ZPC} of the CdSe (pH_{ZPC} = 8.1). In fact, when pH_{ZPC} > pH, the surface charge of CdSe is positive and vice versa at pH_{ZPC} < pH, the surface charge of CdSe is negative. Therefore, CdSe absorbs MB as a cationic dye at pH above 8.1. This is due to the electrostatic adsorption between the cationic dye and the negatively charged surface CdSe. In the photocatalytic oxidation process (Fig. 6), the photogenerated electrons and holes produce superoxide radicals and hydroxyl radical ions, respectively. Then MB molecules are adsorbed onto the CdSe surface and photogenerated holes initiate the oxidation of MB. Reactive oxygen species (ROS), i.e., O₂^{•-} + h_{vb}⁺ + OH^{•-}, decompose MB to minerals as Eqs. (3–6)²⁶:



However, the presence of many hydroxyl ions in an alkaline solution causes the formation of abundant hydroxyl radicals and as a result, causes more degradation of MB at higher pHs. On the other hand, at acidic pH, electrostatic repulsion between positive

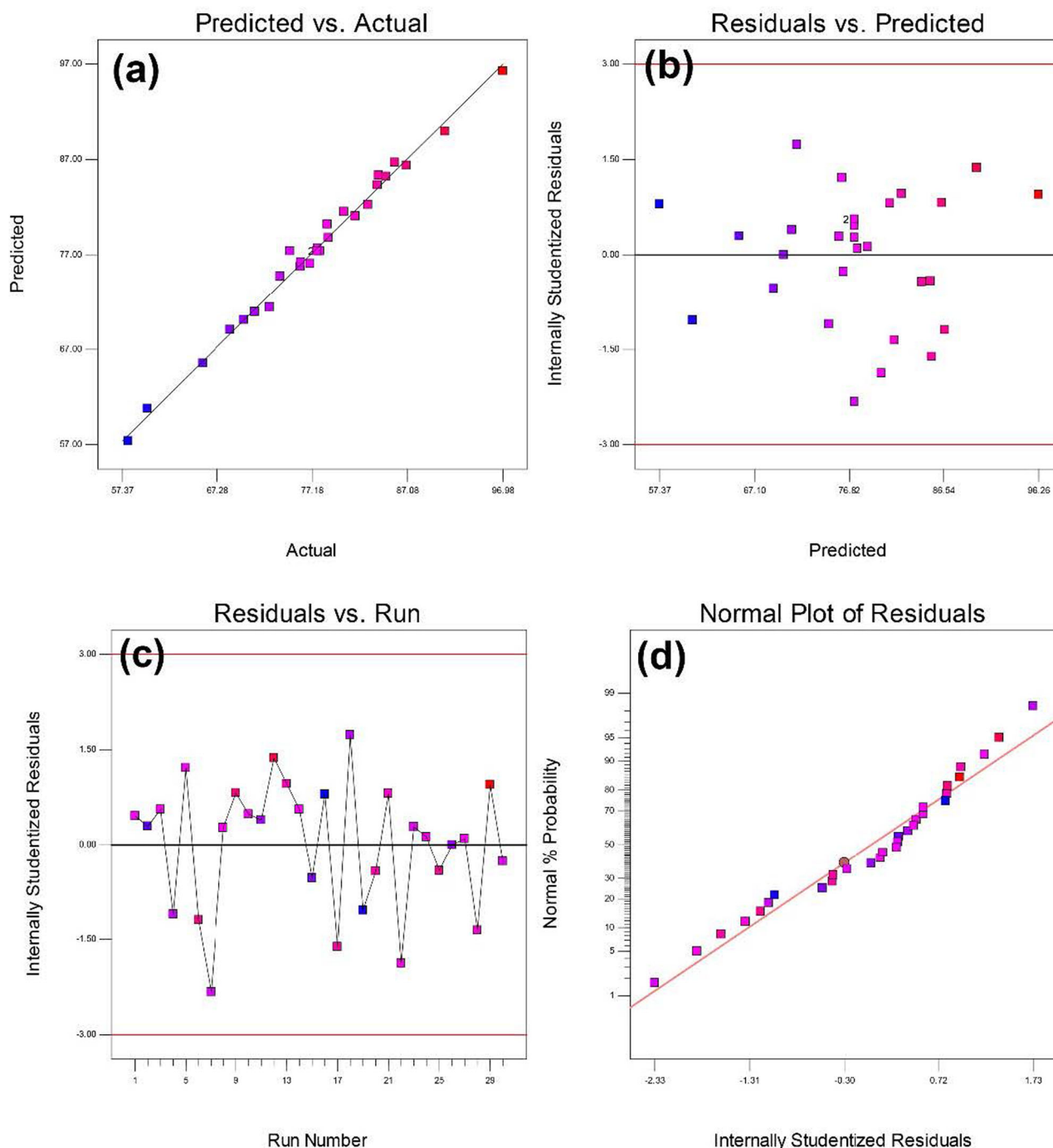


Fig. 4 Statistical plots for Methylene Blue removal by CdSe. **a** Plots of actual values versus predicted ones. **b** The Internally Studentized Residuals versus predicted ones. **c** The Internally Studentized Residuals versus run number. **d** Normal plot of residuals.

surface charges of CdSe and MB molecules reduces the adsorption of MB on the surface of CdSe nanoparticles. In addition, the high amount of produced H^+ at acidic conditions reduced percent hydroxyl radicals and reduced the degradation percentage²⁷.

Optimization

From an economic point of view, optimization of photocatalytic degradation conditions of MB can be achieved by considering independent variables (MB concentration, initial pH, irradiation time, and photocatalyst dosage) and removal efficiency as maximum using Design-Expert® Version 11 Software. The predicted

of MB removal was 92.80% under following conditions: pH = 8, MB concentration = 20 mgL^{-1} , CdSe dosage = $0.02 \text{ g } 50 \text{ mL}^{-1}$ and irradiation time = 20 min. On the other hand, the experimental result of MB removal was about 90.87%, which implies a performance design by RSM.

Usability and stability of the photocatalyst

The usability and stability of the photocatalyst are important for long-term applications. Photocatalyst particles are recovered by centrifuge and collected for new cycles. The reusable performance of CdSe for ten MB degradation cycles (20 mg L^{-1}) was investigated

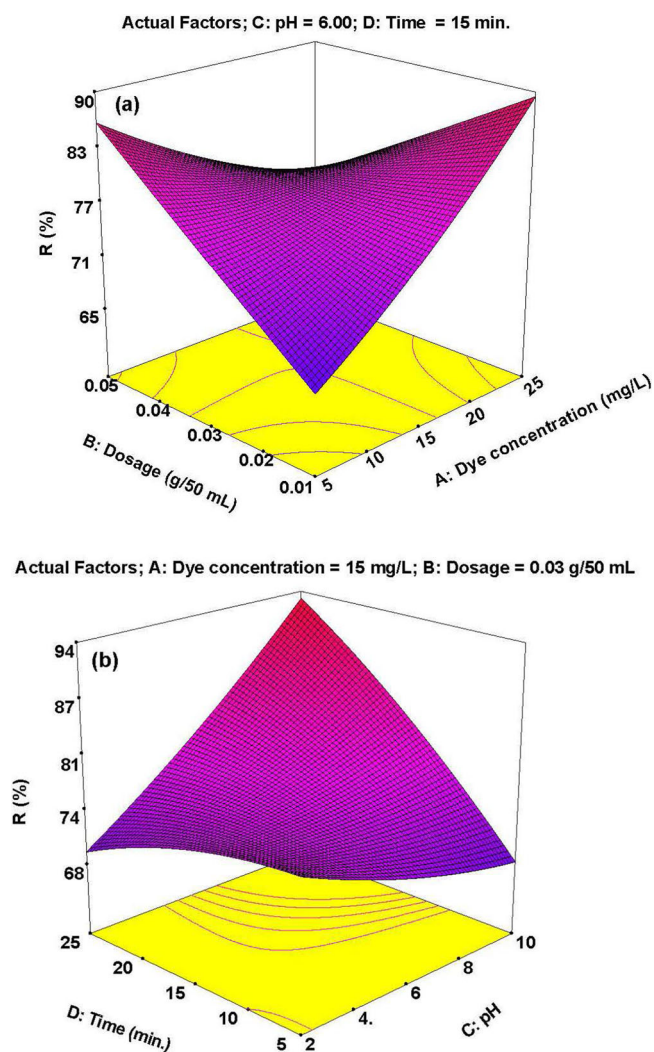


Fig. 5 3D plots of MB photocatalytic degradation interactions. **a** Photocatalyst dosage vs. Dye concentration. **b** Irradiation time vs. pH.

(Supplementary Fig. 3). After ten cycles, the photocatalytic activity of CdSe decreased from 89.87% to 58.76% (31.11%). This decrease in photocatalytic activity can be attributed to the following reasons: (1) Some photocatalyst may be lost during the recovery phase (washing and drying), which reduces the efficiency in the next cycle and thus reduces the catalytic activity of the surface. (2) The catalytic surface activity of the photocatalyst gradually decreased after each cycle due to the blockage of pores and active sites by MB and its intermediates²⁸.

Kinetics

A Langmuir-Hinshelwood (L-H) kinetic model (Eq. 7) was used to describe the photocatalytic degradation kinetics of MB by plotting of $\ln(C/C_0)$ versus time⁵. Where C_0 and C are the MB concentrations in solution at initial any time, respectively, and k is the pseudo-first-order rate constant. The obtained value of k (0.038 min^{-1}) along with the correlation constants ($R^2 = 0.994$) is calculated for the kinetic photodegradation of MB.

$$\ln \frac{C_0}{C} = -kt \quad (7)$$

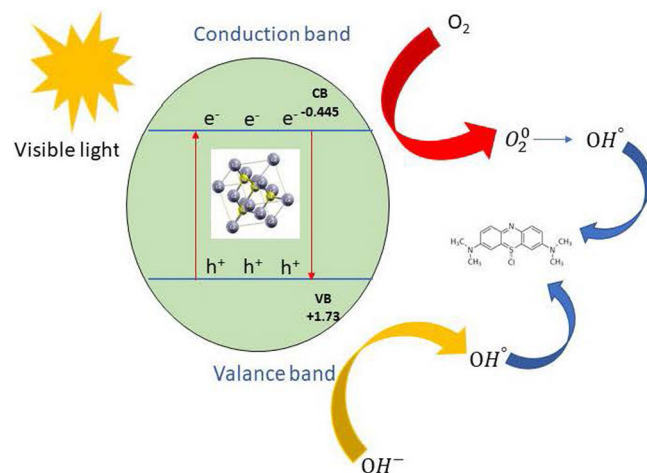


Fig. 6 The proposed mechanism for photodegradation of MB.

Thermodynamic

In order to study the thermodynamics of the photocatalytic process, enthalpy changes (ΔH°), entropy changes (ΔS°) and Gibbs free energy (ΔG°) were obtained using the Eqs. (8–10).

$$K_C = \frac{q_e}{C_e} \quad (8)$$

$$\ln K_C = -\frac{\Delta H^\circ}{R} \left(\frac{1}{T} \right) + \frac{\Delta S^\circ}{R} \quad (9)$$

$$\Delta G^\circ = -RT \ln K_C \quad (10)$$

Here, R ($8.314 \text{ J mol}^{-1} \text{ K}^{-1}$) is the universal gas constant, T (K) is temperature and K_C (mL g^{-1}) is the equilibrium constant of reaction and is obtained from Eq. 9. By plotting the $\ln K_C$ in terms of $1/T$ (van Hoff diagram) and obtaining the line equation, the ΔH° and ΔS° values can be calculated using the slope and intercept of the diagram, respectively (Supplementary Fig. 4). ΔG° can be calculated at the desired temperatures using Eq. 10²⁹. Thermodynamic variables were calculated at different temperatures and the results were collected in Supplementary Table 3. A negative ΔG° indicates that the adsorption process is spontaneous and feasible in nature²⁹. Also, a positive ΔH° value confirmed that this reaction is endothermic in nature. In general, ΔH° between 2.1 and 20.9 kJ mol^{-1} indicates physical adsorption, while values between 80 and 200 kJ mol^{-1} confirm chemical adsorption³⁰. In this study, the value of ΔH° was obtained at $17.96 \text{ kJ mol}^{-1}$ that indicates that photocatalytic degradation of MB is a physical process. Also, the positive ΔS° confirmed the increase in randomness on the liquid-solid interface during the photocatalytic degradation process. This revealed the photocatalytic removal process is performed through the electrostatic connection between the MB and CdSe and via physical adsorption. Also, a positive ΔS° showed a high affinity for MB adsorption onto the CdSe resulting in high degradation efficiency.

The activation energy of all photocatalytic process was measured by Arrhenius equation (Eq. 11)²⁹:

$$k = A \exp \left(-\frac{E_a}{RT} \right) \quad (11)$$

Here, A , R , T , k , and E_a represent the frequency factor, gas constant ($\text{J mol}^{-1} \text{ K}^{-1}$), solution temperature (K), rate constant, and activation energy (J mol^{-1}), respectively. This represents the minimum energy required to complete the photocatalytic reaction. Activation energy indicates a physical or chemical process of degradation. Low activation energies (0 to 40 kJ mol^{-1}) indicate a physical adsorption process, while higher activation energies (40 to

800 kJmol⁻¹) indicate a chemical adsorption process³¹. The value of E_a is obtained at 13.896 kJmol⁻¹, i.e., <40 kJmol⁻¹, which indicated the photocatalytic degradation of MB occurs via the physical process.

Scavengers

The effects of scavengers including isopropanol (hydroxyl radicals scavenger), chloride (hole scavenger), ascorbic acid (superoxide scavenger), and nitrate (electron scavenger)³² on photocatalytic degradation of MB (20 mg L⁻¹) was investigated at pH = 8. The results are compared in Supplementary Fig. 5. A comparison between the activities of the scavenging agents confirms that the greatest reduction in the photocatalytic activity of CdSe is achieved by chloride ions and isopropanol. This process confirms that the photogenerated holes and hydroxyl radicals are the most important than the superoxide and electrons in the photocatalytic degradation of MB.

METHODS

Materials

Selenium powder, Methylene Blue, hydrochloric acid, and Sodium hydroxide were purchased from Merck Company. Cadmium nitrate, ethylenediamine (EDA), and polyvinyl pyrrolidone (PVP) were prepared from Sigma-Aldrich.

Preparation of CdSe

Typically, 0.0315 g of Se (0.4 mmol) was dissolved in 80 ml of EDA at 200 °C for 2 h until the black color appeared (sample A). In another flask, 2 g of polyvinylidene pyrrolidone was dissolved in 70 ml of distilled water as a capping agent and was stirred at 70 °C for 150 min. to obtain homogeneous solutions (sample B). Then 0.094 g of Cd(NO₃)₂ · 4H₂O (0.4 mmol) and selenium ethylenediamine (sample A) were added into the PVP solution (sample B) to make a homogeneous solution while stirring. The obtained solution was left to dry at 70 °C and was crushed by a mortar until it became powder. Then it was calcinated in a tube furnace at 500 °C under a flow of nitrogen at 50 cm³ min⁻¹ for 90 min²².

Response surface methodology model

RSM is a technique that is widely used mathematical and statistical methods for optimization of specific response influenced by variables³³. In fact, relationships between response and input factors are determined by RSM³⁴. In RSM, the selection of levels is crucial for any factor. The level of each factor should also be coded on a +/-1 basis for good regression analysis. For this, Eq. 12 can be used:

$$X = \frac{x - \frac{[x_{\max} + x_{\min}]}{2}}{\frac{[x_{\max} - x_{\min}]}{2}} \quad (12)$$

Where, X is the factor code, x represents the actual factor value, and x_{\min} and x_{\max} are the minimum and maximum factor values, respectively^{18,35}. The experimental design was performed based on Design-Expert® Version 11 Software using RSM. The effect of four independent factors including initial MB concentration, pH of the solution, irradiation time, and photocatalyst dosage were considered at five levels (-2, -1, 0, 1, 2). A second-order polynomial equation is used to study the effect of independent variables on MB removal (Eq. 13):

$$y = \beta_0 + \sum_{i=1}^k \beta_i x_i + \sum_{i=1}^k \beta_{ii} x_i^2 + \sum_{i=1}^k \sum_{j \neq i}^k \beta_{ij} x_i x_j \quad (13)$$

Here, y is the predicted responses, β_0 , β_i , β_{ii} & β_{ij} are constant, linear effect, square effect, and interaction effect coefficients, respectively, and x_i and x_j refer to independent variables.

Photocatalytic experiments

Then photocatalytic experiments were performed on a 100 ml crystallizer containing 0.01–0.05 g 50 ml⁻¹ of photocatalyst with various concentrations of MB. Also, photocatalytic experiments were performed with tungsten-halogen lamps (300 watts) with a UV cut filter (>420 nm). The mixture was sonicated for 10 min. before the lamp was turned on.

Then, the lamp was turned on to start the photocatalytic degradation of MB. After the reactions were completed, the samples were filtered, and adsorption of total solutions was recorded at a maximum wavelength of 664 nm using a UV-Vis spectrophotometer³⁶. Equation (14) was used to calculate the MB removal:

$$R(\%) = \frac{[C]_0 - [C]_t}{[C]_0} \times 100 \quad (14)$$

[C]₀ is initial and [C]_t is at any time concentration of MB (mg L⁻¹), respectively.

The Debye-Scherrer Eq. (15) was used to estimate the size of CdSe particles, where D is the particle size; K is constant (0.89), λ is the wavelength of radiation (1.5406 Å); β is the full width at half maximum of the peak and θ is the diffracted angle of the peak³⁷.

$$D = \frac{K\lambda}{\beta \cos \theta} \quad (15)$$

The average size of prepared CdSe has obtained about 70 nm that was in good agreement with FESEM results. Also, the theoretical density of prepared CdSe was calculated from Eq. (16):

$$\rho = \frac{8M}{Na^3} \quad (16)$$

Where, ρ is theoretical density, N is Avogadro number, M is the molecular mass of the sample, and "a" is the lattice parameter³⁸. Determination of specific surface area is a significant parameter in adsorption, heterogeneous catalysis, and surface reactions. Sauter's Eq. (17) is used to calculate of the specific surface area of the sample.

$$\text{specific surface area} = \frac{6000}{\rho \times D} \quad (17)$$

Where, ρ and D are theoretical density and particle size of the sample, respectively.

Stability and reusability

The stability and reusability of CdSe in the batch system were evaluated in 10 cycles. The precipitated catalyst was washed with deionized water in each experiment and dried at 50 °C for reuse.

Analytical procedure

The analytical procedure of synthesized CdSe nanoparticles is presented in Text 1 s.

DATA AVAILABILITY

All data generated or analysed during this study are included in this published article (and its Supplementary Information files).

Received: 7 March 2022; Accepted: 15 July 2022;

Published online: 08 August 2022

REFERENCES

- Malefane, M. E. et al. In-situ synthesis of Tetraphenylporphyrin/Tungsten (VI) Oxide/Reduced Graphene Oxide (TPP/WO₃/RGO) nanocomposite for visible light photocatalytic degradation of Acid Blue 25. *Chemistry Select* **7**, 8379 (2019).
- Shamsi Kasmaei, A., Rofouei, M. K., Olya, M. E. & Ahmed, S. Kinetic and thermodynamic studies on the reactivity of hydroxyl radicals in wastewater treatment by advanced oxidation processes. *Prog. Color. Color. Coat.* **13**, 1 (2020).
- Seifpanahi-Shabani, K., Eyvazkhani, A. & Heidari, P. Bioremediation of textile dyes wastewater: potential of bacterial isolates from a mining soils and wetlands. *Prog. Color. Color. Coat.* **12**, 155 (2019).
- Bhattacharyya, K. G. & Sharma, A. Kinetics and thermodynamics of methylene blue adsorption on neem (Azadirachta indica) leaf powder. *Dye. Pigment.* **65**, 51–59 (2005).
- Akyüz, D. rGO-TiO₂-CdO-ZnO-Ag photocatalyst for enhancing photocatalytic degradation of methylene blue. *Opt. Mater. (Amst.)* **116**, 111090 (2021).
- Mafa, P. J. et al. Cobalt oxide/copper bismuth oxide/samarium vanadate (Co₃O₄/CuBi₂O₄/SmVO₄) dual Z-scheme heterostructured photocatalyst with high

- charge-transfer efficiency: Enhanced carbamazepine degradation under visible light irradiation. *J. Colloid Interface Sci.* **603**, 666 (2021).
7. Al-Momani, F., Touraud, E., Degorce-Dumas, J. R., Roussy, J. & Thomas, O. Biodegradability enhancement of textile dyes and textile wastewater by VUV photolysis. *J. Photochem. Photobiol. A Chem.* **153**, 191 (2002).
 8. Sabzehmeidani, M. M., Karimi, H. & Ghaedi, M. Visible light-induced photo-degradation of methylene blue by n-p heterojunction CeO₂/CuS composite based on ribbon-like CeO₂ nanofibers via electrospinning. *Polyhedron* **170**, 160 (2019).
 9. Danish, M. S. S. et al. Photocatalytic applications of metal oxides for sustainable environmental remediation. *Met. (Basel)* **11**, 80 (2021).
 10. Mukherjee, A. & Ghosh, S. Absorption spectra of CdSe–ZnS core–shell quantum dots at high photon energies: experiment and modeling. *Phys. E Low-Dimensional Syst. Nanostruct.* **64**, 234 (2014).
 11. Michalet, X. et al. Quantum dots for live cells, in vivo imaging, and diagnostics. *Science* **307**, 538 (2005).
 12. Ghosh, T. et al. Graphene oxide based CdSe photocatalysts: synthesis, characterization and comparative photocatalytic efficiency of rhodamine B and industrial dye. *Mater. Res. Bull.* **48**, 1268 (2013).
 13. Song, C., Li, X., Wang, L. & Shi, W. W. Fabrication, characterization and response surface method (RSM) optimization for tetracycline photodegradation by Bi₂S₃/GO. 24-graphene oxide (BWO-GO). *Sci. Rep.* **18**, 1 (2016).
 14. Abdullah, A. H., Moey, H. J. & Yusof, N. A. Response surface methodology analysis of the photocatalytic removal of Methylene Blue using bismuth vanadate prepared via polyol route. *J. Environ. Sci.* **24**, 1694 (2012).
 15. Popoola, L. T. Nano-magnetic walnut shell-rice husk for Cd (II) sorption: design and optimization using artificial intelligence and design expert. *Heliyon* **5**, e02381 (2019).
 16. Ávila-López, M. A., Luévano-Hipólito, E. & Torres-Martínez, L. M. Optimizing the CO₂ reduction to produce CH₃OH using flexible NiMoO₄ coatings as a photocatalyst. *J. Alloy. Compd.* **21**, 165549 (2022).
 17. Dalanta, F., Kusworo, T. D., Aryanti, N. & Othman, N. H. Optimization of AC/TiO₂/CeO₂ composite formulation for petroleum refinery wastewater treatment via simultaneous adsorption-photocatalytic process using D-optimal mixture experimental design. *J. Environ. Chem. Eng.* **1**, 106517 (2021).
 18. Almeida, L. C., Gasparotto, L. H. S., Bocchi, N., Rocha-Filho, R. C. & Biaggio, S. R. Galvanostatic Pb (II) removal from a simulated wastewater by using a stainless-steel wool cathode in a flow-through cell: a factorial-design study. *J. Appl. Electrochem.* **38**, 167 (2008).
 19. Makwakwa, T., Mafa, P., Nyoni, H., Msagati, T. Optimization of square wave voltammetry (SWV) parameters by design of experiment (DOE) methodologies for the determination of mifepristone at glassy carbon electrode (GCE). *Electroanalysis*, In press.
 20. Al-Hada, N. M. et al. A facile thermal-treatment route to synthesize the semiconductor CdO nanoparticles and effect of calcination. *Mater. Sci. Semicond. Process.* **26**, 460 (2014).
 21. Al-Hada, N. M. et al. A facile thermal-treatment route to synthesize ZnO nanosheets and effect of calcination temperature. *PLoS One* **9**, e103134 (2014).
 22. Salem, A. et al. Synthesis and characterization of CdSe nanoparticles via thermal treatment technique. *Results Phys.* **7**, 1556 (2017).
 23. Rahimi, B., Jafari, N., Abdolhnejad, A., Farrokhzadeh, H. & Ebrahimi, A. Application of efficient photocatalytic process using a novel BiVO₄/TiO₂-NaY zeolite composite for removal of acid orange 10 dye in aqueous solutions: Modeling by response surface methodology (RSM). *J. Environ. Chem. Eng.* **7**, 103253 (2019).
 24. Vaez, Z. & Javanbakht, V. Synthesis, characterization and photocatalytic activity of ZSM-5/ZnO nanocomposite modified by Ag nanoparticles for methyl orange degradation. *J. Photochem. Photobiol. A Chem.* **388**, 112064 (2020).
 25. Sajjadi, S., Khataee, A. & Kamali, M. Sonocatalytic degradation of methylene blue by a novel graphene quantum dots anchored CdSe nanocatalyst. *Ultrason. Sonochem.* **39**, 676 (2017).
 26. Lopes, P. A. L., de, D. L., Maia, S. & Silva, L. A. Chalcogenide nanoparticles like CdxZn(1-x)SySe(1-y) applied to photocatalytic hydrogen production from natural seawater under visible light irradiation. *Mater. Today Commun.* **25**, 101503 (2020).
 27. Khataee, A. et al. Sonochemical synthesis of Pr-doped ZnO nanoparticles for sonocatalytic degradation of Acid Red 17. *Ultrason. Sonochem.* **22**, 371 (2015).
 28. Moosavi, S. et al. Methylene blue dye photocatalytic degradation over synthesised Fe₃O₄/AC/TiO₂ nano-catalyst: degradation and reusability studies. *Nanomaterials* **10**, 2360 (2020).
 29. Zulficar, M., Samsudin, M. F. R. & Sufian, S. Modelling and optimization of photocatalytic degradation of phenol via TiO₂ nanoparticles: an insight into response surface methodology and artificial neural network. *J. Photochem. Photobiol. A Chem.* **384**, 112039 (2019).
 30. Liu, Y. Is the free energy change of adsorption correctly calculated. *J. Chem. Eng. Data.* **54**, 1981 (2009).
 31. Keerthana, B. G. T., Solaiyammal, T., Muniyappan, S. & Murugakoothan, P. Hydrothermal synthesis and characterization of TiO₂ nanostructures prepared using different solvents. *Mater. Lett.* **220**, 20 (2018).
 32. Ghattavi, S. & Nezamzadeh-Ejehieh, A. A double-Z-scheme ZnO/Ag/WO₃ photocatalyst with high visible light activity: experimental design and mechanism pathway in the degradation of methylene blue. *J. Mol. Liq.* **322**, 114563 (2021).
 33. Montgomery, D. C. *Design and analysis of experiments*, John Wiley & sons (2017).
 34. Said, K. A. M. & Amin, M. A. M. Overview on the response surface methodology (RSM) in extraction processes. *J. Appl. Sci. Process Eng.* **2**, 170 (2015).
 35. Lucas, J. M. Response surface methodology: process and product optimization using designed experiments. *J. Qual. Technol.* **42**, 228 (2010).
 36. Mosavi, S. A., Ghadi, A., Gharbani, P. & Mehrizad, A. Photocatalytic removal of Methylene Blue using Ag@ CdSe/Zeoilte nanocomposite under visible light irradiation by Response Surface Methodology. *Mater. Chem. Phys.* **267**, 124696 (2021).
 37. Amiri, F., Dehghani, M., Amiri, Z., Yousefinejad, S. & Azhdarpoor, A. Photocatalytic degradation of 2, 4-dichlorophenoxyacetic acid from aqueous solutions by Ag₃PO₄/TiO₂ nanoparticles under visible light: kinetic and thermodynamic studies. *Water Sci. Technol.* **83**, 3110 (2021).
 38. Chahar, D. et al. Photocatalytic activity of cobalt substituted zinc ferrite for the degradation of methylene blue dye under visible light irradiation. *J. Alloy. Compd.* **851**, 156878 (2021).

AUTHOR CONTRIBUTIONS

P.G.: Conceptualization, Methodology, Formal analysis, Writing-review & editing. A.M.: Funding Acquisition, Project Administration, Writing-review & editing. S.A.M.: Methodology.

COMPETING INTERESTS

The authors declare no competing interests.

ADDITIONAL INFORMATION

Supplementary information The online version contains supplementary material available at <https://doi.org/10.1038/s41545-022-00178-x>.

Correspondence and requests for materials should be addressed to Parvin Gharbani.

Reprints and permission information is available at <http://www.nature.com/reprints>

Publisher's note Springer Nature remains neutral with regard to jurisdictional claims in published maps and institutional affiliations.



Open Access This article is licensed under a Creative Commons Attribution 4.0 International License, which permits use, sharing, adaptation, distribution and reproduction in any medium or format, as long as you give appropriate credit to the original author(s) and the source, provide a link to the Creative Commons license, and indicate if changes were made. The images or other third party material in this article are included in the article's Creative Commons license, unless indicated otherwise in a credit line to the material. If material is not included in the article's Creative Commons license and your intended use is not permitted by statutory regulation or exceeds the permitted use, you will need to obtain permission directly from the copyright holder. To view a copy of this license, visit <http://creativecommons.org/licenses/by/4.0/>.

© The Author(s) 2022